Synthesis and formation mechanism of TiO_2/SnO_2 composite nanobelts by electrospinning

CHAO SONG, XIANGTING DONG*
School of Chemistry and Environmental Engineering Changchun University of Science and Technology, Changchun, 130022, P.R. of China

PVP/[$Ti(SO_4)_2$+$SnCl_4$] composite nanobelts were prepared via electrospinning, and TiO_2/SnO_2 composite nanobelts were fabricated by calcination of the prepared composite nanobelts. The samples were characterized by thermogravimetric-differential thermal analysis (TG-DTA), X-ray diffractometry (XRD), Fourier transform infrared spectroscopy (FTIR), and Scanning electron microscopy (SEM). XRD results show that the composite nanobelts were amorphous in structure, and pure phase TiO_2/SnO_2 composite nanobelts were obtained by calcination of the relevant composite nanobelts at 750 ºC for 8 h, the structure of TiO_2/SnO_2 composite nanobelts was tetragonal with space group *$P4_2/mnm$*. SEM analysis indicates that the surface of as-prepared composite nanobelts was smooth, the widths of the composite fibers were in narrow range, and the mean width was *ca.* 11.766±1.607 μm, thickness was about 161 nm, and there is no cross-linking among nanobelts. The width of TiO_2/SnO_2 composite nanobelts was *ca.* 2.831±0.909 μm, the thickness of TiO_2/SnO_2 composite nanobelts was about 57.8 nm. TG-DTA analysis reveals that the DMF, organic compounds and inorganic salts in the composite nanobelts were decomposed and volatilized totally, and the weight of the sample kept constant when sintering temperature was above 750 ºC, and the total weight loss percentage was 82%. FTIR analysis manifests that crystalline TiO_2/SnO_2 composite nanobelts were formed at 750 ºC. The possible formation mechanism of the TiO_2/SnO_2 composite nanobelts was preliminarily discussed.

(Received October 22, 2011; accepted November 23, 2011)

Keywords: TiO_2/SnO_2, Composite nanobelts, Electrospinning, Formation mechanism

1. Introduction

Fujishima and Honda [1-3] discovered the phenomenon of photocatalytic splitting of water on a TiO_2 electrode under ultraviolet light since 1972, enormous efforts have been devoted to the research of TiO_2 materials, which has led to many promising applications in sunscreens [4-5], paints [6], ointments [7-8], toothpastes [9], solar cells [10-12] and photocatalysis [13]. In recent years, researchers have started to focus on TiO_2 nanobelts. For instance, Kai Pan [14] et al. synthesized TiO_2 belts using the hydrothermal method. To the best of our knowledge, there have been no reports on the preparation and properties of TiO_2/SnO_2 nanobelts. Electrospinning is a simple and convenient method for the preparation of one-dimensional nanomaterials. Various belts such as GGG:Eu^{3+} [15], PANI [16], three mixed oxides [17] have been fabricated by electrospinning. In this paper, metallic chlorides and sulfates were used as raw materials, PVP was used as template and DMF as solvent. PVP/[$Ti(SO_4)_2$+$SnCl_4$] precursor composite nanobelts were fabricated by electrospinning and TiO_2/SnO_2 composite nanobelts were prepared by calcination of the relevant precursor composite nanobelts. The structure and morphology of the TiO_2/SnO_2 composite nanobelts were systematically investigated.

2. Experimental section

2.1 Preparation of PVP/[$Ti(SO_4)_2$+$SnCl_4$] precursor composite sol

Precursor solution was prepared by dissolving $SnCl_4 \cdot 5H_2O$ and $Ti(SO_4)_2$ in DMF. An amount of poly(vinyl pyrrolidone) (PVP, M_w=90,000) was added into the above solution, followed by stirring for 8 h at room temperature and then remaining motionlessly for 3 h. Then the PVP/[$Ti(SO_4)_2$+$SnCl_4$] precursor composite sol was obtained.

2.2 Preparation of TiO_2/SnO_2 composite nanobelts

Schematic diagram of electrospinning setup was shown in Fig. 1. The above precursor sol was placed in a syringe and delivered at a constant flow rate using a plastic capillary. The anode was placed in the sol, and a grounded aluminum foil served as counter electrode and collector. When a high voltage (15 kV in this work) was applied, and the distance between the capillary tip and the collector was fixed to 19-21 cm, a dense web of PVP/[$Ti(SO_4)_2$+$SnCl_4$] precursor composite nanobelts was collected on the aluminum foil. These belts were calcinated at a rate of 1 ºC/min and remained for 8 h at 750 ºC, respectively. Thus,

TiO_2/SnO_2 composite nanobelts were obtained.

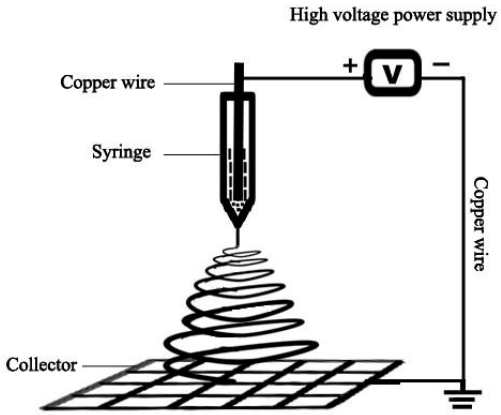

Fig.1. Schematic diagram of electrospinning setup for preparation of composite nanobelts.

2.3 Characterization methods

XRD analysis was performed on a Holland Philip Analytical PW1710 BASED X-ray diffractometer using Cu $K\alpha_1$ radiation, with the working current and voltage at 30 mA and 40 kV, respectively. Scans were made from 10 ° to 90 ° at the speed of 4 (°)/min, and the step was 0.02 °. The morphology and size of the samples were observed with an S-4200 scanning electron microscope made by Japanese Hitachi Company. TG-DTA analysis was carried out on an SDT-2960 thermal analyzer made by American TA instrument company in atmosphere, and the temperature rising rate was 10 °C/min. FTIR spectra of the samples were recorded on BRUKER Vertex 70 Fourier transform infrared spectrophotometer made by Germany Bruker company, and the specimen for the measurement was prepared by mixing the sample with KBr powders and then the mixture was pressed into pellets, the spectrum was acquired in a wave number range from 4000 cm^{-1} to 400 cm^{-1} with a resolution of 4 cm^{-1}.

3. Results and discussion

3.1 TG-DTA analysis

Fig. 2 shows the thermal behavior of PVP/[$Ti(SO_4)_2$+$SnCl_4$] precursor composite nanobelts. The weight loss was involved in four stages in TG curve. The first weight loss is 9% in the range of 40 to 100 ºC accompanied by a small endothermic peak near 79 ºC in the DTA curve, which is caused by the loss of the surface absorbed water or the residual water molecules in the precursor composite nanobelts. The second weight loss step (37%) between 100 ºC and 345 ºC were due to the degradation of the main and side chain of PVP, confirmed by two wide exothermic peak near 263 ºC and 340 ºC in the DTA curve. The third weight loss (31%) in the TG curve (345-530 ºC) was possibly corresponded to the decomposition of chlorides and sulfates. In the DTA curve, an exothermic peak was located at 478ºC. The last weight loss (5%) in the TG curve (530-750 ºC) was possibly corresponded to the decomposition of inorganic salts. In the DTA curve, an exothermic peak was located at 734 ºC. And above 750 ºC, the TG and DTA curves were all unvaried, indicating that water, organic compounds and inorganic salts in the precursor composite nanobelts were completely volatilized and pure TiO_2/SnO_2 composite nanobelts could be obtained above 750 ºC. The total weight loss was 82%.

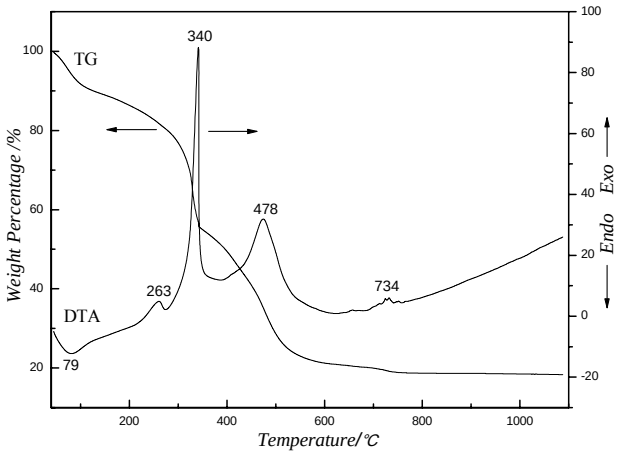

Fig. 2. TG-DTA curves of precursor composite nanobelts.

3.2 XRD analysis

In order to investigate the variety of phase, the PVP/[$Ti(SO_4)_2$+$SnCl_4$] precursor composite nanobelts and samples obtained after being calcined at different temperatures were characterized by XRD, as indicated in Fig. 3. Precursor composite nanobelts (Fig. 3a) only have a broad peak around 20°, which is the typical peak of the polymer [18]. This revealed that precursor composite nanobelts were amorphous in structure. From Fig. 3b, XRD patterns displayed some new diffraction peaks when calcined at 750 ℃, and meanwhile, the diffraction peak of precursor composite material disappeared, indicating that PVP was decomposed and removed out from precursor composite nanobelts, observed reflections were indexed to (110), (101) and (211) of TiO_2, and the *d* values and relative intensity of the peaks are consistent with those of JCPDS standard card (21-1276); and observed reflections can be indexed to (110), (101) and (211) of SnO_2, and the *d* values and relative intensity of the peaks are consistent with those of JCPDS standard card (41-1445). Therefore, TiO_2/SnO_2 composite nanobelts with stable phase can be prepared at 750 ℃.

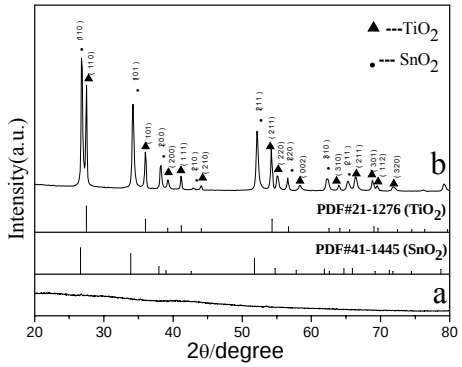

Fig. 3. XRD patterns of the precursor composite nanobelts (a) and samples calcined at 750 ℃ for 8 h (b).

3.3 FTIR spectra analysis

As seen form Fig. 4a, the FTIR spectrum of PVP/[$Ti(SO_4)_2$+$SnCl_4$] precursor composite nanobelts indicated that the wide absorption peak at 3390 cm^{-1} attributes to the stretching vibrations of O-H of the surface absorbed water [19]. The absorption peaks at 2930 cm^{-1}, 1636 cm^{-1}, 1447 cm^{-1}, 1284 cm^{-1} and 1016 cm^{-1} corresponding to the stretching vibrations of C-H, C=O, C-N, C-C and C-H bond in PVP [20-21]. It can be seen from Fig. 4b (750 ℃) that the wide absorption peak at 3444 cm^{-1} of the surface absorbed water became weaker and all peaks of PVP disappeared. At the same time, two new absorption peaks at low wavenumber are appeared, the wide absorption peak at 539 cm^{-1}, which ascribe to the vibration of Ti-O-Ti bonds, the wide absorption peak at 682 cm^{-1}, which ascribe to the vibration of Sn-O bond [22], indicating that the formation of TiO_2/SnO_2 composite nanobelts. The results of FTIR analysis were in good agreement with XRD results.

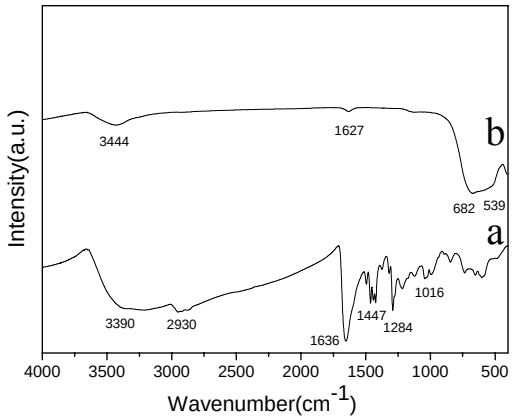

Fig. 4. FTIR spectra of the precursor composite nanobelts (a) and samples calcined at 750 ℃ for 8 h (b).

3.4 SEM and distribution histograms analysis

The morphology of the precursor composite nanobelts and TiO_2/SnO_2 composite nanobelts were investigated by SEM and distribution histograms analysis. As seen from Fig. 5a~5b, the surface of the PVP/[$Ti(SO_4)_2$+$SnCl_4$] precursor composite nanobelts is very smooth. The width of the precursor composite nanobelts is ca. 11.766±1.607 μm (Fig. 6a) and the thickness is about 161 nm. The TiO_2/SnO_2 composite nanobelts became coarser, narrower and thinner with the increase of calcination temperatures, caused by the decomposition of PVP, chlorides and sulfates. The width of composite nanobelts calcined at 750 ℃ (Fig. 5c~5d) is *ca.* 1.861±0.067 μm (Fig. 6b) and the thickness is about 57.8 nm.

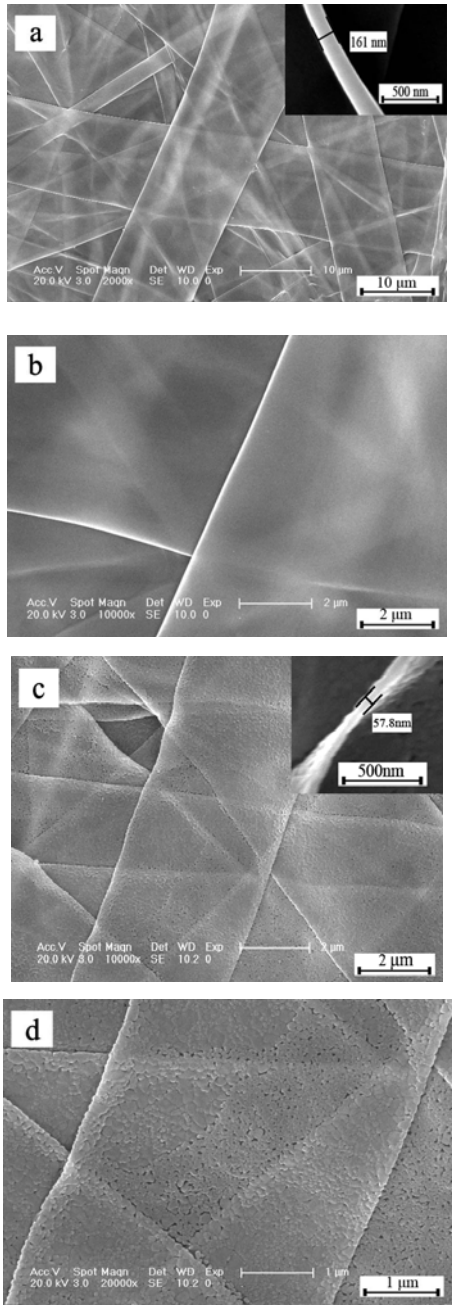

Fig. 5. SEM images of the precursor composite nanobelts (a and b) and samples calcined at 750 ℃ for 8 h (c and d).

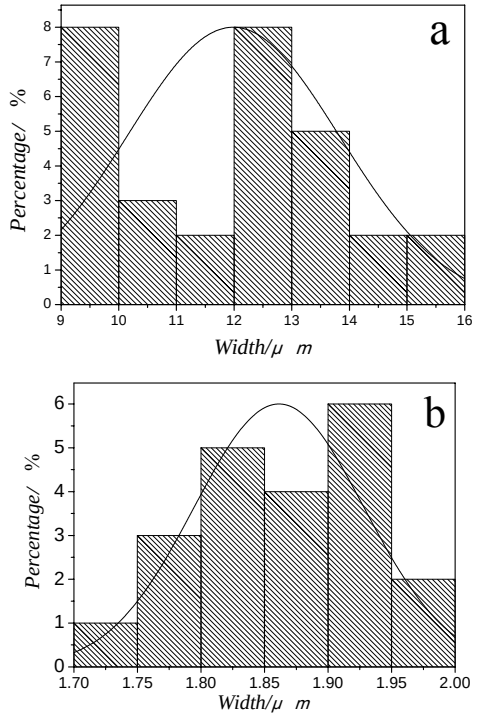

Fig. 6. Width distribution histograms of the precursor composite nanobelts (a) and samples calcined at 750 ℃ for 8 h (b).

3.5 EDS analysis

To determine the composite nanobelts component further, energy dispersive spectroscopy (EDS) of the samples was performed. The EDS analysis results revealed that by calcining the precursor composite nanobelts (Fig. 7a) at 750 ℃ for 8 h the TiO_2/SnO_2 composite nanobelts (Fig. 7b) are only composed of Ti, Sn and O elements. The results of EDS analysis were in good agreement with the above results.

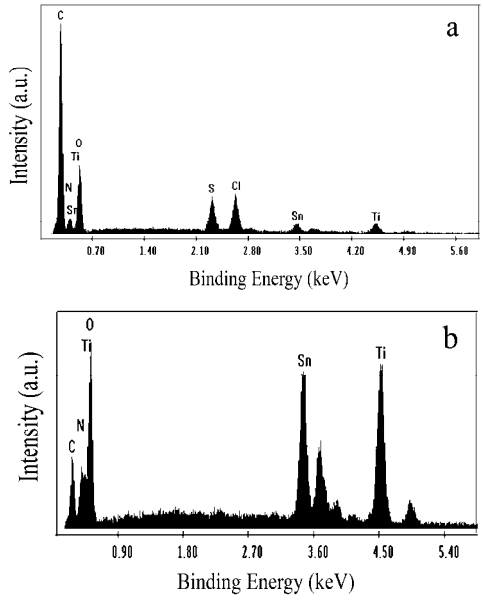

Fig. 7. EDS images of the precursor composite nanobelts (a) and samples calcined at 750 ℃ for 8 h (b).

3.6 Formation mechanism of TiO_2/SnO_2 composite nanobelts

The formation mechanism of TiO_2/SnO_2 composite nanobelts is presented in Fig. 7. Mixed PVP, Ti^{4+}, SO_4^{2-}, Sn^{4+}, NO_3^-, and DMF underwent electrospinning under high voltage to form PVP/[$Ti(SO_4)_2$+$SnCl_4$] precursor composite nanobelts. DMF and Ti^{4+}, SO_4^{2-}, Sn^{4+}, Cl^- were mixed with PVP or adsorbed on the PVP molecules. As the TiO_2/SnO_2 composite nanobelts were formed, PVP played the role of oriented template. Every band in the precursor composite nanobelts of the Ti and Sn ions were limited and located mainly along the length of the precursor composite nanobelts, with a less radial distribution along the precursor composite nanobelts. When the precursor composite nanobelts were heat-treated in solvents, they inclined towards surface diffusion and evaporation; PVP fracture, volatile oxidation, and Cl^-, SO_4^{2-} oxidative decomposition were observed. The thermal motion shortened the distance between the metal ions and the Ti and Sn ions in the air oxidation of TiO_2 and SnO_2 nanocrystals, causing the nanocrystals to combine and form nanoparticles. At high temperature, the solutions within the nanoparticles stretched along the original direction of the precursor composite nanobelts connected with one another, eventually forming TiO_2/SnO_2 composite nanobelts. Further work is under way.

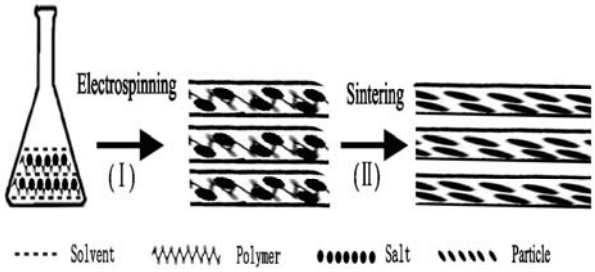

Fig. 7. Illustrative diagram of formation mechanism of composite nanobelts.

4. Conclusions

PVP/[$Ti(SO_4)_2$+$SnCl_4$] precursor composite nanobelts were successfully fabricated using an electrospinning technique, and TiO_2/SnO_2 composite nanobelts were synthesized by calcining the precursor composite nanobelts at 750 °C for 8 h. TG-DTA and FTIR revealed that the formation of TiO_2/SnO_2 composite nanobelts was largely influenced by the calcination temperatures. SEM micrographs indicated that the surface of the precursor composite nanobelts was smooth and became coarse with the increase of calcination temperatures. EDS analysis results revealed that TiO_2/SnO_2 composite nanobelts were only composed of O, Sn and Ti elements.

Acknowledgments

This work was financially supported by the National Natural Science Foundation of China (NSFC 50972020), the Science and Technology Development Planning Project of Jilin Province (Grant Nos. 20070402, 20060504), Key Research Project of Science and Technology of Ministry of Education of China (Grant No. 207026), the Science and Technology Planning Project of Changchun City (Grant No. 2007045) and the Scientific Research Planning Project of the Education Department of Jilin Province (under grant Nos. 2007-45, 2005109).

References

[1] A. Fujishima, K. Honda, Nature, **238**, 37 (1972).
[2] A. Fujishima, T. N. Rao, D. A. Tryk, J. Photochem. Photobiol. C, **1**(1), 1 (2000).
[3] D. A. Tryk, A. Fujishima, K. Honda, Electrochim. Acta, **45**, 2363 (2000).
[4] A. Salvador, M. C. Pascual-Martí, J. R. Adell, A. Requeni, J. G. March, Journal of Pharmaceutical and Biomedical Analysis, **22**(2), 301 (2000).
[5] R. Zallen, M. P. Moret, Solid State Commun, **137**(3), 154 (2006).
[6] J. H. Braun, A. Baidins, R. E. Marganski, Prog. Org. Coat, **20**(22), 105 (1992).
[7] Xiaobo Chen, Samuel S. Mao, Chem. Rev, **107**, 2891 (2007).
[8] D. V. Bavykin, J. M. Friedrich, F. C. Walsh, Adv. Mater, **18**, 2807 (2006).
[9] S. A. Yuan, W. H. Chen, S. S. Hu, Mater. Sci. Eng. C, **25**, 479 (2005).
[10] DaeUn Lee, SongRim Jang, R. Vittal, Jiwon Lee, KangJin Kim, Solar Energy, **82**, 1042 (2008).
[11] Bin Liu, Eray S. Aydil, J. Am. Chem. Soc, **131**, 3985 (2009).
[12] Jinting Jiu, Seiji Isoda, Fumin Wang, Motonari Adachi, J. Phys. Chem. B, **110**, 2087 (2006).
[13] Ramya Chandrasekar, Lifeng Zhang, Jane Y. Howe Nyle E. Hedin. Yan Zhang, Hao Fong, J. Mater Sci., **44**, 1198 (2009).
[14] Kai Pan, Qinglin Zhang, Qiang Wang, Zhaoyue Liu, Dejun Wang, Jinghong Li, Yubai Bai, Thin Solid Films, **515**, 4085 (2007).
[15] Liu Ying, Wang Jing-Xian, Dong Xiang-Ting, et al. Chemical Journal of Chinese Universities, **31**, 1291 (2010).
[16] Qiao Zhen Yu, Ying Li, Mang Wang, Hong Zheng Chen. Chinese Chemical Letters, **19**, 223 (2008).
[17] Muzafar A. Kanjwal, Nasser A. M. Barakat, Faheem A. Sheikh, Myung Seob Khil, Hak Yong Kim. J Mater Sci., **43**, 5489 (2008).
[18] JiunYu Chen, HungCheng Chen, JiunNan Lin, Changshu Kuo, Materials Chemistry and physics, **107**, 480 (2008).
[19] Remant, Bahadur, K, C.; Chul, Ki, Kim.; Myung, Seob, Khil.; Hak, Yong, Kim.; Ick, Soo, Kim. Mater. Sci. Eng. C., **28**, 70 (2008).
[20] B. Ding, H. Kim, C. Kim, M. Khil, S. Park, Nanotechnology, **14**, 532 (2003).
[21] M. I. Baraton, L. Merhari, J.-Z. Wang, K. E. Gonsalves, Nanotechnology **9**, 356 (1998).
[22] Kaile Wang, Bolun Yang, Yu Liu, Chunhai Yi, Energy Fuels, **23**, 4209 (2009).

*Corresponding author: songchaocc@126.com